Received: 17 June 2020 | Revised: 9 September 2020 | Accepted: 21 October 2020

DOI: 10.1002/sia.6906

SPECIAL ISSUE ARTICLE

SURFACE and INTERFACE ANALYSIS WILEY

An in situ exploration of subsurface defect migration to a liquid water-exposed rutile TiO_2(110) surface by XPS

M. H. Mesbah Ahmed | Robert H. Temperton | James N. O'Shea

School of Physics & Astronomy, University of Nottingham, Nottingham, UK

Correspondence
James N. O'Shea, School of Physics & Astronomy, University of Nottingham, Nottingham NG7 2RD, UK.
Email: J.Oshea@nottingham.ac.uk

Funding information
Engineering and Physical Sciences Research Council, Grant/Award Number: Doctoral Prize; Innovate UK, Grant/Award Number: ERA; University of Nottingham, Grant/Award Number: Propulsion Futures Beacon

The ability of titanium dioxide to split water into OH^- and H^+ species is heavily dependent on the behaviour of defects in the crystal structure at or near the surface. We present an in situ study of defect migration in rutile TiO_2(110) conducted using X-ray photoelectron spectroscopy (XPS). First, surface and subsurface defects were created in the crystal by argon ion sputtering. Subsequent in situ exposure of the defective crystal to liquid water healed the surface defects, whereas the subsurface remained defective. The sample was then annealed while XPS was used to monitor the concentration of titanium defects. At low annealing temperatures, Ti^{3+} was observed to migrate from the subsurface to the surface. Further annealing gradually restored the surface and subsurface to the defect-free Ti^{4+} form, during which the changes in abundance of Ti^{1+}, Ti^{2+} and Ti^{3+} defects are discussed.

KEYWORDS
ambient pressure XPS, defects, titanium dioxide, water, X-ray photoelectron spectroscopy

1 | INTRODUCTION

The production of hydrogen through photocatalytic water splitting is an appealing next-generation energy technology with potential to provide a low-cost, sustainable and environmentally responsible fuel.[1,2] For an overview of photocatalysis, we would direct the reader to one of the many recent review articles on the topic.[3–6] This paper discusses titanium dioxide, an attractive photocatalyst due to its chemical stability, abundance and nontoxicity and has been widely considered as a candidate not only for water splitting[7] but also water purification[8,9] and numerous other photocatalytic applications.[10] Further, titanium dioxide is well suited to being sensitised with dye molecules to increase visible light absorption[11] or can be doped to modify photocatalytic properties,[12] for example, stabilising reactive facets on the surface of the catalyst.[13] The catalytic activity of titania depends heavily on the surface crystallinity. For anatase, the photocatalytic activity can be tuned by the exposure of (101) and (001) facets, which act as reduction and oxidation sites, respectively.[14] The rutile (110) surface, which although not as catalytically active as anatase, can be used to split water and produce stoichiometric quantities of hydrogen and oxygen.[15]

As part of the effort to develop suitable photoelectrodes for water splitting, single-crystal surfaces have been extensively studied in an attempt to better understand the fundamental surface chemistry governing catalytic performance.[16–19] The structure of the rutile titanium dioxide (110) surface is shown in Figure 1. The bulk crystal consists of sixfold coordinated titanium atoms and threefold coordinated oxygen atoms, but at the (110) surface, there is additionally rows of twofold coordinated oxygen, located at the bridge sites running in the [001] direction and fivefold coordinated titanium.[20,21] It is now well understood that defects in the crystal structure play a critical role in the photocatalytic performance of titanium dioxide. For example, the defect-free rutile TiO_2 surface does not dissociate/split water.[22,23] Water splitting on the rutile surface is instead largely dictated by oxygen vacancies in the rows of bridging oxygen atoms and is often dependent on the nature and density of these surface defect sites.[24–27] The dissociation of a water molecule into H^+ and OH^- occurs near an oxygen vacancy site where the OH group fills an

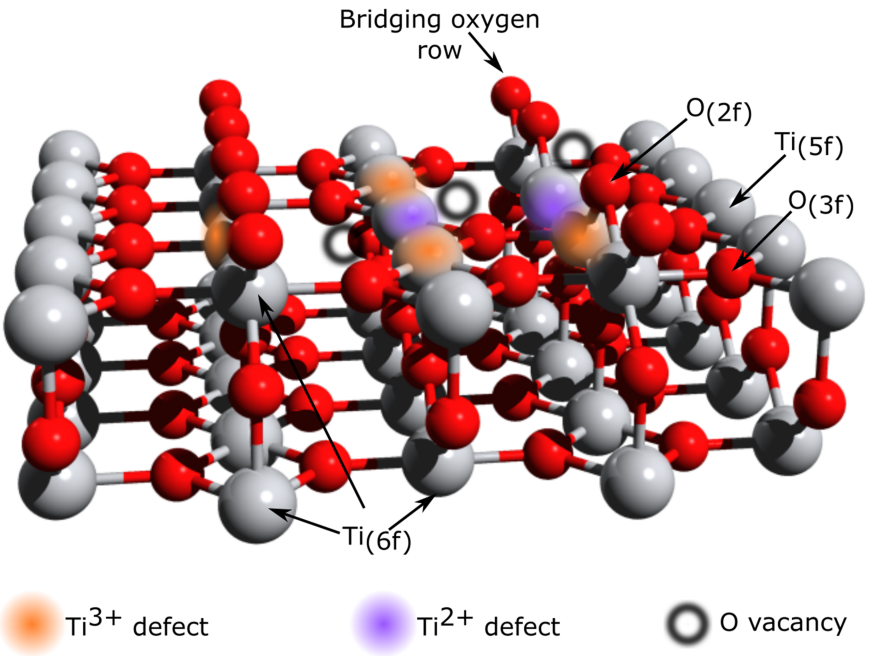

FIGURE 1 The rutile TiO_2(110) surface, which in the defect-free form consist of fivefold and sixfold coordinated Ti environments ($Ti_{(5f)}$ and $Ti_{(6f)}$) with corresponding twofold and threefold coordinated oxygen environments ($O_{(2f)}$ and $O_{(3f)}$). Examples of oxygen vacancies, both in a bridging oxygen row and in the main crystal structure, are highlighted alongside corresponding Ti defects

oxygen vacancy (V_{bridge}) and the H binds to a nearby bridging oxygen site (O_{bridge}) forming an additional OH species on the surface. This mechanism can be outlined as follows:

$$H_2O + V_{bridge} + O_{bridge} \rightarrow 2OH_{bridge}. \quad (1)$$

Defects in TiO_2(110) can be easily prepared by Ar^+ ion sputtering, which damages the crystallinity and preferentially removes oxygen atoms from both the crystal surface and subsurface layers.[28] The resulting reduced titania mainly consists of two types of defect: oxygen vacancies (missing atoms from the bridging oxygen rows) and titanium interstitials (titanium atoms not assigned to a lattice point that can move through the crystal).[20] After sputtering, it is well known that the defect-free rutile structure can be restored by annealing in vacuum. This process is entirely reliant on the mobility of the defects, which can be explained through two mechanisms. First, during 'oxygen vacancy diffusion', the undamaged crystal bulk supplies O^{2-} anions to the reduced surface/subsubsurface. Second, 'Ti^{3+} interstitial diffusion' describes the bulk receiving excess Ti^{3+} species from the surface/subsurface. In both cases, the migration of defects to and from the bulk allows the defect-free rutile structure to be restored.[28]

Given the importance of defect chemistry on the catalytic activity of titania, it is not surprising that the interaction between water and defective titanium dioxide surfaces has been extensively studied using an array of techniques.[26,29-34] In particular, near-ambient pressure X-ray photoelectron spectroscopy (NAP-XPS) is particularly well suited having been used to study the role of oxygen vacancies as water nucleation sites on rutile[24] and anatase.[35] Current understanding is that oxygen vacancies on the surface of anatase migrate to the subsurface[35] where they are more stable and less reactive.[36] Water dissociation occurring on the surface is enhanced at sites above a subsurface defect, which causes the binding to be more favourable.[37] This differs from rutile where oxygen defects are more common on the surface (compared with the subsurface), where they are stable and tend to remain.[35,38] Water dissociation on rutile occurs directly at these surface oxygen vacancies.[39] This difference, which has also been studied computationally,[40] is thought to explain the relatively increased catalytic reactivity of the anatase polymorph compared with rutile as the defects, which can trap photoexcited charge carriers, are not so easily quenched by adsorbates, including water, if they remain subsurface.

In this study, highly defective rutile TiO_2(110) was prepared by Ar^+ sputtering; the surface of which was healed in situ by exposure to liquid water in a NAP-XPS instrument. The resulting combination of a defect-free surface and highly defective subsurface is used as a platform for an XPS study of annealing-induced defect migration.

2 | METHOD

Measurements were taken using a SPECS DeviSim NAP-XPS instrument consisting of an ultra-high vacuum (UHV) preparation/analysis chamber and interchangeable NAP cells that can be docked onto the entrance of the Phoibos 150 NAP hemispherical analyser. Using this arrangement, described elsewhere,[41] samples can be transferred between the NAP cell and the UHV chamber without breaking vacuum. The NAP cell used was equipped with a Peltier thermoelectric heater/cooler providing precise control of the sample temperature, in the $\sim \pm 50^{\circ}$C range, via a proportional integral derivative (PID) controller and a thermocouple mounted between on the sample plate beneath the crystal.

A rutile TiO_2(110) crystal (PI-KEM Ltd.) was cleaned in the UHV chamber by rounds of 1-kV argon ion sputtering and 800-K annealing

until no evidence of contamination or surface defects were visible in the XPS. The sample was then sputtered at 2 kV for 10 min to create a highly defective surface and subsurface. The crystal was then transferred into the NAP cell where it was cooled to 275 K before 6 mbar of water (deionised using a Triple Red purification system and further degassed by freeze pump thaw cycles) was introduced. This pressure and temperature combination, corresponding to 100% relative humidity, produced a liquid film of water on the surface. After liquid water exposure, the NAP cell was pumped down and the sample returned to the UHV chamber (base pressure in the low 10^{-10} mbar range) where the sample was annealed in situ using an electron beam heater behind the sample plate. The temperature during annealing was measured using a thermocouple located at the edge of the sample plate (~3 mm from the edge of the sample).

XPS was measured with a pass energy of 20 eV in the UHV chamber and 40 eV in the NAP cell. The geometry of the NAP cell allowed measurement at normal emission (NE). Measurements in UHV were taken at both NE (0°) and 70° grazing emission (GE). Monochromatic Al Kα X-rays (hν = 1486.6 eV) were used for all measurements and the binding energy scale was calibrated using the oxide lattice O 1*s* peak previously measured to have a binding energy of 530.05 eV.[42] Peak fitting was performed using a pseudo-Voigt line shape with a fixed Lorentzian width (0.3 eV) and variable Gaussian width after the subtraction of a Shirley background.[43]

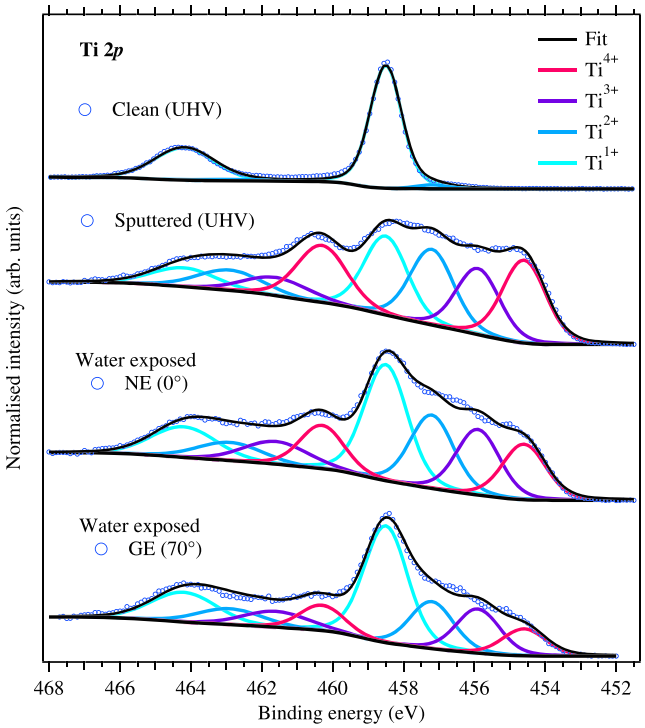

FIGURE 2 Ti 2*p* XPS of 'clean' (after UHV cleaning/annealing), 'sputtered' (after 2-keV Ar^+ sputtering) and 'water-exposed' (after liquid water exposure) surfaces where peak fitting tracks the behaviour of the Ti oxidation states. All three surfaces were measured in normal emission (NE). Additionally, the 'water-exposed' surface was measured at the more surface-sensitive angle of 70° grazing emission (GE)

3 | RESULTS AND DISCUSSION

Figure 2 shows Ti 2*p* XPS measurements of rutile TiO_2(110) after three successive surface preparations/modifications: 'clean' (after UHV cleaning as described above), 'sputtered' (after 2-keV Ar^+ sputtering) and 'water exposed' (returned to UHV after liquid water exposure). The 'clean' spectrum shows a doublet attributed to Ti^{4+} with a trace of residual Ti^{3+} defects, which are visible as a shoulder at the lower binding energy side of Ti^{4+}.[20] After sputtering, a complex series of lower binding energy features are present in the spectra (sputtered) extending down to ~453 eV, which we have curve fitted to four spin–orbit doublets attributed to lower Ti oxidation states (Ti^{3+}, Ti^{2+}, Ti^{1+}) formed by the removal of oxygen atoms producing defects that extend nanometres into the surface.[25,44] This highly defective sample was subsequently exposed to liquid water with the aim of healing the defects at the very surface of the crystal (the in situ data collected during this process are included in the supporting information). The resulting spectrum (water-exposed NE) in Figure 2 shows that the additional Ti oxidation states decrease in relative intensity. This preparation method repeatedly produced very similar defect concentrations; measurements showing this repeatability are included in the supporting information.

The surface sensitivity of XPS can be varied by changing the angle of the sample with respect to the spectrometer.[45] We predict the escape depth of Ti 2*p* photoelectrons at NE (0°) and GE (70°) to be ~7 and ~2 nm, respectively, calculated by considering the inelastic mean free path (IMFP) needed to attenuate the substrate signal by 95% (method described elsewhere[46]). The NE and GE traces in Figure 2 therefore indicate that the water-exposed surface is less defective than the bulk as, when compared with the NE data, the more surface-sensitive GE spectrum (water-exposed GE) shows fewer defect states relative to the Ti^{4+}. This conclusion is consistent with an independent study where defects at the surface were healed more readily than those subsurface.[47] The defect states are not expected to disappear completely in the GE spectrum presented in Figure 2 as the calculated information depth is still ~2 nm and it is assumed that water exposure only heals defects directly accessible on the surface.

Annealing this 'water-healed' sample in UHV produces the data shown in Figure 3, which provides information about how the defect states change as a function of time and temperature. During the first 3 min of annealing, the defect states increase in intensity. After which we see the defect concentration slowly diminish until the spectrum is dominated by Ti^{4+}, which has occurred by the time the temperature approaches 700 K.

For better understanding, five individual spectra have been extracted from Figure 3 at points labelled (a)–(e). These are plotted, alongside the corresponding O 1*s* spectra, in Figure 4 where curve fitting allows the spectral contribution of the different Ti oxidation states to be determined. The peak located at 458.5 eV corresponds to the Ti $2p_{3/2}$ of the Ti^{4+} oxidation state.[48] The three peaks located at 457.2, 455.9 and 454.6 eV are attributed to the Ti^{3+}, Ti^{2+} and Ti^{1+} oxidation states, respectively. The corresponding Ti $2p_{1/2}$ components were determined in the fitting procedure; a fixed spin–orbit splitting

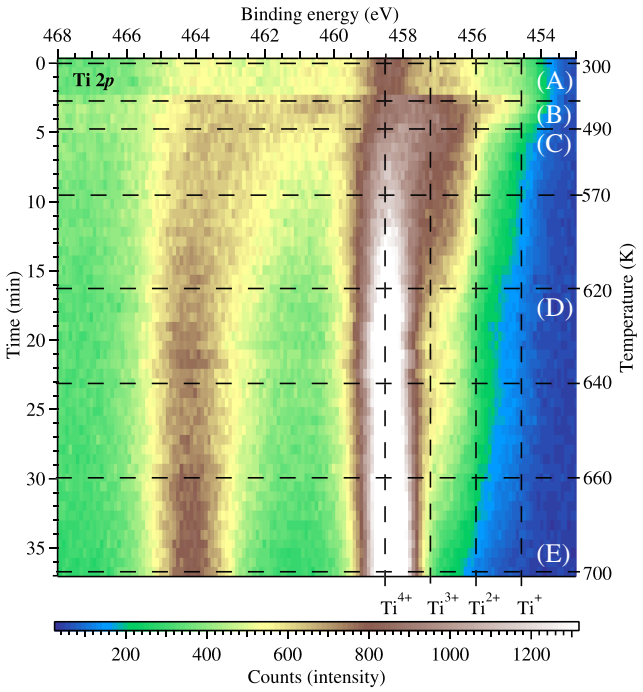

FIGURE 3 Normal emission Ti 2*p* XPS measured in situ during annealing of 'water-exposed' rutile TiO_2 (110). Horizontal lines labelled (a)—(e) were extracted for detailed analysis in Figure 4

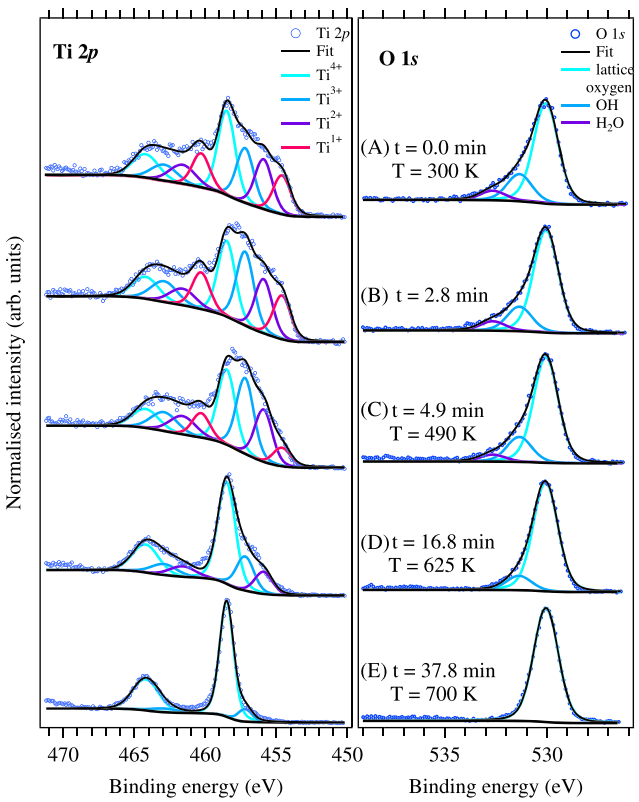

FIGURE 4 Left: Ti 2*p* spectra (extracted from Figure 3) where peak fitting tracks the behaviour of the Ti oxidation states during annealing. Right: associated O 1*s* spectra highlighting the relative change of lattice oxygen, hydroxyl groups and adsorbed water. All the spectra were measured at normal emission

of 5.70 eV led to Ti $2p_{1/2}$ components with relative areas of 0.45 ± 0.03 compared with the corresponding Ti $2p_{3/2}$ components. The Ti^{3+}, Ti^{2+} and Ti^{1+} peaks are likely to be broadened with a rather complex line shape due to multiplet splitting.[49] We have opted to keep the peak fitting as simple as possible and not modelled the multiplet splitting, which in reality will lead to an asymmetric broadening of the Ti^{3+}, Ti^{2+} and Ti^{1+} on the higher BE side and the intensity of the multiplet peak is likely very small in comparison with the main peak so likely only makes a small difference to the quantitative analysis we present. During the first ~3 min, the features attributed to Ti^{3+} are observed to grow during annealing as shown in Figure 4a,b. Beyond this point, starting from $t \approx 5$ min (Figure 4c, 490 K), the intensity of the lower oxidation states has decreased and continues to decrease as time elapses and the temperature increases.

The O 1*s* spectra in Figure 4 are fitted with three peaks. The peak at 530.05 eV is attributed to lattice oxygen, whereas the features located at 1.3 and 2.6 eV higher binding energy correspond to adsorbed hydroxide and water, respectively. The relative positions of these features are consistent with a previous study of a water-exposed rutile TiO_2(110) surface.[24] The intensity of the adsorbed hydroxide and water features remains comparable during the first two spectra (a,b). In spectrum c, at $t \approx 5$ min and $T \approx 490$ K, we start to see a loss of absorbed water. By the fourth spectra d at $t \approx 17$ min and $T \approx 620$ K, the water is no longer observed and the OH peak has started to diminish. Finally, by $t \approx 38$ min and $T \approx 700$ K (spectrum e), we see no hydroxide or absorbed water features. This is consistent with previous measurements of water-exposed TiO_2 surfaces showing that hydroxide and adsorbed water do not desorb below 550 K.[47] It is noteworthy that we do not see a reduction of the hydroxide/water features at lower temperatures perhaps implying that the water is not playing a dramatic role healing any Ti^{3+} defects that may have migrated to the surface, potentially as physisorbed water is not kinetically active enough when compared with the gas and liquid phases, which are known to heal defects.

Figure 5 quantitatively shows how the relative concentration of the different titanium oxidation states changes during annealing (plotted as a function of time and temperature). The plot has been split into three regions, labelled A to C, to aid discussion. We do emphasise, however, that the boundaries between these regions are likely not distinct and the mechanisms dominating the behaviour in the regions may overlap. The entire experiment, where we healed the defective surface through water exposure followed by tracking the defects while annealing, was repeated with in situ XPS measurements at a more surface-sensitive grazing emission angle. These data are included in the supporting information for comparison, showing the same trends in defect concentrations occurring at similar temperatures.

In region A, that is, during the first ~3 min, Figure 5 shows a decrease in Ti^{4+} concentration with a corresponding increase in Ti^{3+}, whereas the contribution of lower oxidation states remains constant. This implies that at low annealing temperatures, Ti^{3+} defects are likely diffusing from the subsurface to the surface until the concentration

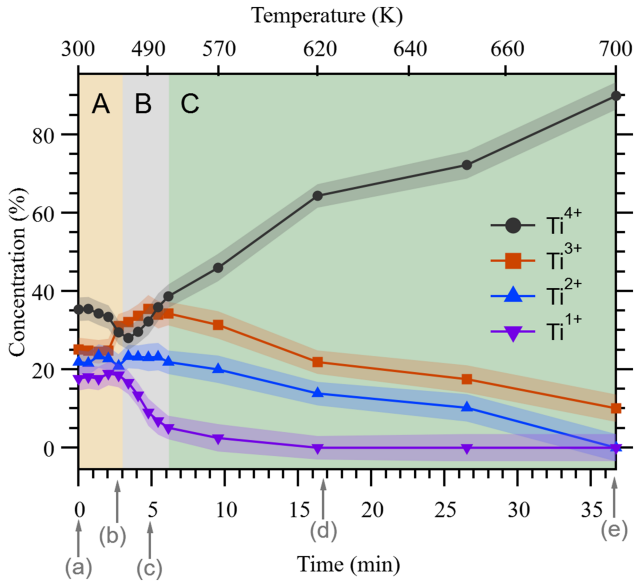

FIGURE 5 Defect concentration, extracted from peak fitting of Ti 2*p* normal emission XPS data (examples in Figure 4) as a function of time and temperature. Shaded regions around the data points indicate an estimated error bar calculated from the standard deviation of the fit residual. Regions A to C represent stages of the annealing process as discussed in the text. Arrow indicated label (a)–(e) corresponds to the spectra presented in Figure 4

gradient between the surface and subsurface is minimised as the Ti^{4+} reaches a minima at ~3 min.

In region B, between ~3 and ~6 min, we observe that the Ti^{1+} concentration dramatically decrease, whereas the Ti^{3+} and Ti^{4+} increase proportionally. The Ti^{2+} component remains constant. This could perhaps be consistent with progressive conversion of $Ti^{1+} \rightarrow Ti^{2+} \rightarrow Ti^{3+} \rightarrow Ti^{4+}$ if the $Ti^{1+} \rightarrow Ti^{2+}$ and $Ti^{2+} \rightarrow Ti^{3+}$ conversions have comparable rates; alternatively, intermediate oxidation states may be skipped. Regardless, region B represents a dramatic transition with an activation energy corresponding to a temperature of ~490 K where Ti^{1+} is no longer stable.

In region C, beyond ~6 min, the Ti^{1+} concentration approaches 0%, the Ti^{2+} and Ti^{3+} begin to gradually and constantly decline at a comparable rate, whereas the Ti^{4+} increases accordingly (with a slower rate than in region B). We attribute this regime to the gradual diffusion of oxygen vacancies and Ti interstitials between the crystal bulk and surface/subsurface layers eventually resulting in a essentially defect free spectrum. Towards the higher annealing temperatures, where the bridging oxygen atoms are no longer hydrogen terminated, it is possible that residual water in the vacuum chamber may contribute to the healing of surface defects via the water dissociation mechanisms discussed in Section 1.[31,34,50]

Although it appears notable that the rapid depletion of Ti^{1+} observed in region B is not observed for Ti^{2+} or Ti^{3+}, it is worth emphasising that the rate of heating is much greater at the start of annealing; to an approximation, the temperature change during regions A and B (~6 min) is comparable with the ~30 min elapsed in region C. The results presented here are therefore unable to separate the effects of annealing temperature and time. We therefore suggest that there would be great value in an investigation of the phenomena observed here using an instrument designed for accurate temperature-controlled XPS measurements to disentangle the thermodynamics from the kinetics and provide more accurate transition temperatures. In addition, a similar study on anatase, where it is favourable for defects to remain subsurface, would make an interesting comparison.

4 | CONCLUSIONS

Defective rutile TiO_2(110), prepared using Ar^+ sputtering, was exposed to liquid water, which hydroxylates the surface oxygen vacancies created by sputtering. The result was a sample with a highly defective subsurface coexisting with a defect free surface, providing a platform for annealing-induced migration of titanium defects to be studied using XPS. We observe at low annealing temperatures an increase in Ti^{3+} concentration, which is attributed to migration of Ti^{3+} to the previously defect-free surface. A rapid and distinct depletion of Ti^{1+} is observed around 500 K with a corresponding increase in Ti^{3+} quickly followed by Ti^{4+}, which is tentatively explained by progressive conversion of Ti^{1+} defects to Ti^{4+} via intermediate oxidation states. At higher annealing temperatures, we observe the gradual depletion of the remaining defects, likely through established titanium interstitial and oxygen vacancy diffusion mechanisms. The experimental evidence of defects migrating to the surface of rutile at low annealing temperatures is an important consideration for the industrial application of titania catalysts, and the methodology presented here provides a useful tool for studying the kinetics and thermodynamics of defect migration in a range of materials.

ACKNOWLEDGEMENT

The authors acknowledge and thank Innovate UK through the Energy Research Accelerator, the Engineering and Physical Sciences Research Council (EPSRC), the Bangabandhu Science & Technology Fellowship Trust and the University of Nottingham Propulsion Futures Beacon for funding this research.

ORCID

James N. O'Shea https://orcid.org/0000-0003-4687-7257

REFERENCES

1. Li L, Yan J, Wang T, et al. Sub-10 nm rutile titanium dioxide nanoparticles for efficient visible-light-driven photocatalytic hydrogen production. *Nat Commun*. 2015;6:5881.
2. Wu S, Wang W, Tu W, et al. Premixed stagnation flame synthesized TiO_2 nanoparticles with mixed phases for efficient photocatalytic hydrogen generation. *ACS Sustain Chem Eng*. 2018;6 (11):14470-14479.
3. Djurišić AB, He Y, Ng AMC. Visible-light photocatalysts: prospects and challenges. *APL Mater*. 2020;8(3):30903.
4. Luo H, Zeng Z, Zeng G, et al. Recent progress on metal-organic frameworks based-and derived-photocatalysts for water splitting. *Chem Eng J*. 2020;383:123196.

5. Chen S, Huang D, Xu P, et al. Semiconductor-based photocatalysts for photocatalytic and photoelectrochemical water splitting: will we stop with photocorrosion? *J Mater Chem A*. 2020;8(5):2286-2322.
6. Dai C, Liu B. Conjugated polymers for visible-light-driven photocatalysis. *Energy Environment Sci*. 2020;13:24.
7. Nowotny J, Bak T, Nowotny MK, Sheppard LR. Titanium dioxide for solar-hydrogen I. Functional properties. *Int J Hydro Energy*. 2007;32 (14):2609-2629.
8. Loeb SK, Alvarez PJJ, Brame JA, et al. The technology horizon for photocatalytic water treatment: sunrise or sunset? *Environment Sci Technol*. 2019;53(6):2937-2947.
9. Lee S-Y, Park S-J. TiO_2 photocatalyst for water treatment applications. *J Indust Eng Chem*. 2013;19(6):1761-1769.
10. Fujishima A, Rao TN, Tryk DA. Titanium dioxide photocatalysis. *J Photochemist Photobiol C: Photochemist Rev*. 2000;1(1):1-21.
11. Weston M, Reade TJ, Britton AJ, Handrup K, Champness NR, O'Shea JN. A single centre water splitting dye complex adsorbed on rutile TiO_2(110): photoemission, X-ray absorption, and optical spectroscopy. *J Chem Phys*. 2011;135(11):114703.
12. Kumar SG, Devi LG. Review on modified TiO_2 photocatalysis under uv/visible light: selected results and related mechanisms on interfacial charge carrier transfer dynamics. *J Phys Chem A*. 2011;115(46): 13211-13241.
13. Ruan L, Wang X, Wang T, et al. Surface defect-controlled growth and high photocatalytic H_2 production efficiency of anatase TiO_2 nanosheets. *ACS Appl Mater Interfaces*. 2019;11(40):37256-37262.
14. Kumar SG, Rao KSRK. Comparison of modification strategies towards enhanced charge carrier separation and photocatalytic degradation activity of metal oxide semiconductors (TiO_2, WO_3 and ZnO). *Appl Surface Sci*. 2017;391:124-148.
15. Li R, Weng Y, Zhou X, et al. Achieving overall water splitting using titanium dioxide-based photocatalysts of different phases. *Energy Environ Sci*. 2015;8(8):2377-2382.
16. Yamamoto S, Bluhm H, Andersson K, et al. In situ X-ray photoelectron spectroscopy studies of water on metals and oxides at ambient conditions. *J Phys Condensed Matter*. 2008;20(18):184025.
17. Patrick CE, Giustino F. Structure of a water monolayer on the anatase TiO_2(101) surface. *Phys Rev Appl*. 2014;2(1):14001.
18. Wang CW, Yang S, Fang WQ, Liu P, Zhao H, Yang HG. Engineered hematite mesoporous single crystals drive drastic enhancement in solar water splitting. *Nano Letters*. 2016;16(1):427-433.
19. Yu S, Han B, Lou Y, Qian G, Wang Z. One-step fabrication of highly self-hydroxylated TiO_2 mesocrystals and photocatalytic behavior towards water splitting. *Int J Hydrogen Energy*. 2020;45(7): 4596–4605.
20. Diebold U. The surface science of titanium dioxide. *Surface Sci Rep*. 2003;48(5-8):53-229.
21. Teobaldi G, Hofer WA, Bikondoa O, Pang CL, Cabailh G, Thornton G. Modelling STM images of TiO_2(110) from first-principles: defects, water adsorption and dissociation products. *Chem Phys Lett*. 2007; 437(1-3):73-78.
22. Diebold U. Structure and properties of TiO_2 surfaces: a brief review. *Appl Phys A*. 2003;76(5):681-687.
23. Henderson MA. The interaction of water with solid surfaces: fundamental aspects revisited. *Surface Sci Rep*. 2002;46(1-8):1-308.
24. Ketteler G, Yamamoto S, Bluhm H, et al. The nature of water nucleation sites on TiO_2(110) surfaces revealed by ambient pressure X-ray photoelectron spectroscopy. *J Phys Chem C*. 2007;111(23): 8278-8282.
25. Mayer JT, Diebold U, Madey TE, Garfunkel E. Titanium and reduced titania overlayers on titanium dioxide (110). *J Electron Spectroscopy Related Phenomena*. 1995;73(1):1-11.
26. Serrano G, Bonanni B, Di Giovannantonio M, et al. Molecular ordering at the interface between liquid water and rutile TiO_2(110). *Adv Mater Interfaces*. 2015;2(17):1500246.
27. Schaub R, Thostrup P, Lopez N, et al. Oxygen vacancies as active sites for water dissociation on rutile TiO_2(110). *Phys Rev Letters*. 2001;87 (26):266104.
28. Henderson MA. A surface perspective on self-diffusion in rutile TiO_2. *Surface Sci*. 1999;419(2-3):174-187.
29. Schaefer A, Lanzilotto V, Cappel UB, Uvdal P, Borg A, Sandell A. Defect-induced water bilayer growth on anatase TiO_2(101). *Langmuir*. 2018;34(37):10856-10864.
30. Henderson MA. An hreels and tpd study of water on TiO_2(110): the extent of molecular versus dissociative adsorption. *Surface Sci*. 1996; 355(1-3):151-166.
31. Bikondoa O, Pang CL, Ithnin R, Muryn CA, Onishi H, Thornton G. Direct visualization of defect-mediated dissociation of water on TiO_2(110). *Nat Materials*. 2006;5(3):189-192.
32. Liu L-M, Zhang C, Thornton G, Michaelides A. Structure and dynamics of liquid water on rutile TiO_2(110). *Phys Rev B*. 2010;82(16): 161415.
33. Pan J-M, Maschhoff BL, Diebold U, Madey TE. Interaction of water, oxygen, and hydrogen with TiO_2(110) surfaces having different defect densities. *J Vacuum Sci Technol A: Vacuum Surfaces Films*. 1992;10(4): 2470-2476.
34. Li Y, Gao Y. Interplay between water and TiO_2 anatase (101) surface with subsurface oxygen vacancy. *Phys Rev Lett*. 2014;112(20): 206101.
35. Jackman MJ, Thomas AG, Muryn C. Photoelectron spectroscopy study of stoichiometric and reduced anatase TiO_2(101) surfaces: the effect of subsurface defects on water adsorption at near-ambient pressures. *J Phys Chem C*. 2015;119(24):13682-13690.
36. He Y, Dulub O, Cheng H, Selloni A, Diebold U. Evidence for the predominance of subsurface defects on reduced anatase TiO_2(101). *Phys Rev Lett*. 2009;102(10):106105.
37. Aschauer U, He Y, Cheng H, Li S-C, Diebold U, Selloni A. Influence of subsurface defects on the surface reactivity of TiO_2: water on anatase (101). *J Phys Chem C*. 2010;114(2):1278-1284.
38. Li H, Guo Y, Robertson J. Calculation of TiO_2 surface and subsurface oxygen vacancy by the screened exchange functional. *J Phys Chem C*. 2015;119(32):18160-18166.
39. Brookes IM, Muryn CA, Thornton G. Imaging water dissociation on TiO_2(110). *Phys Rev Lett*. 2001;87(26):266103.
40. Cheng H, Selloni A. Surface and subsurface oxygen vacancies in anatase TiO_2 and differences with rutile. *Phys Rev B*. 2009;79(9):92101.
41. Knudsen J, Andersen JN, Schnadt J. A versatile instrument for ambient pressure X-ray photoelectron spectroscopy: the lund cell approach. *Surface Sci*. 2016;646:160-169.
42. Schnadt J, O'shea JN, Patthey L, et al. Structural study of adsorption of isonicotinic acid and related molecules on rutile TiO_2(110) II: XPS. *Surface Sci*. 2003;544(1):74-86.
43. McCusker CE, Castellano FN. Design of a long-lifetime, earth-abundant, aqueous compatible Cu (i) photosensitizer using cooperative steric effects. *Inorganic Chem*. 2013;52(14):8114-8120.
44. Hashimoto S, Tanaka A. Alteration of Ti 2p xps spectrum for titanium oxide by low-energy ar ion bombardment. *Surface Interface Anal: Int J Devoted Develop Appl Techniq Anal Surfaces Interfaces Thin Films*. 2002;34(1):262-265.
45. Fadley CS. Angle-resolved X-ray photoelectron spectroscopy. *Progress Surface Sci*. 1984;16(3):275-388.
46. Seah MP, Dench WA. Quantitative electron spectroscopy of surfaces: a standard data base for electron inelastic mean free paths in solids. *Surface Interface Anal*. 1979;1(1):2-11.
47. Wang L-Q, Baer DR, Engelhard MH, Shultz AN. The adsorption of liquid and vapor water on TiO_2(110) surfaces: the role of defects. *Surface Sci*. 1995;344(3):237-250.
48. Temperton RH, Gibson A, O'Shea JN. In situ XPS analysis of the atomic layer deposition of aluminium oxide on titanium dioxide. *Phys Chemist Chem Phys*. 2019;21(3):1393-1398.

49. Gupta RP, Sen SK. Calculation of multiplet structure of core p-vacancy levels. II. *Phys Rev B*. 1975;12(1):15.
50. Hussain H, Tocci G, Woolcot T, et al. Structure of a model TiO_2 photocatalytic interface. *Nat Mater*. 2017;16(4):461-466.

SUPPORTING INFORMATION

Additional supporting information may be found online in the Supporting Information section at the end of this article.

How to cite this article: Ahmed MHM, Temperton RH, O'Shea JN. An in situ exploration of subsurface defect migration to a liquid water-exposed rutile TiO_2(110) surface by XPS. *Surf Interface Anal*. 2020;1–7. https://doi.org/10.1002/sia.6906